PHILOSOPHICAL TRANSACTIONS OF THE ROYAL SOCIETY A

CrossMark click for updates

Phil. Trans. R. Soc. A (2012) **370**, 4958–4971
doi:10.1098/rsta.2012.0201

Towards electrical spin injection into $LaAlO_3$–$SrTiO_3$

By M. Bibes*, N. Reyren, E. Lesne, J.-M. George, C. Deranlot, S. Collin, A. Barthélémy and H. Jaffrès

Unité Mixte de Physique CNRS-Thales, 1 Avenue Augustin Fresnel, 91767 Palaiseau, France and Université Paris-Sud, 91405 Orsay, France

Future spintronics devices will be built from elemental blocks allowing the electrical injection, propagation, manipulation and detection of spin-based information. Owing to their remarkable multi-functional and strongly correlated character, oxide materials already provide such building blocks for charge-based devices such as ferroelectric field-effect transistors (FETs), as well as for spin-based two-terminal devices such as magnetic tunnel junctions, with giant responses in both cases. Until now, the lack of suitable channel materials and the uncertainty of spin-injection conditions in these compounds had however prevented the exploration of similar giant responses in oxide-based lateral spin transport structures. In this paper, we discuss the potential of oxide-based spin FETs and report magnetotransport data that suggest electrical spin injection into the $LaAlO_3$–$SrTiO_3$ interface system. In a local, three-terminal measurement scheme, we analyse the voltage variation associated with the precession of the injected spin accumulation driven by perpendicular or longitudinal magnetic fields (Hanle and 'inverted' Hanle effects). The spin accumulation signal appears to be much larger than expected, probably owing to amplification effects by resonant tunnelling through localized states in the $LaAlO_3$. We give perspectives on how to achieve direct spin injection with increased detection efficiency, as well on the implementation of efficient top gating schemes for spin manipulation.

Keywords: oxide interfaces; spin injection; spintronics

1. Introduction

In many oxide systems, several energy scales strongly compete to determine the ground state, leading to a rich variety of phases depending on internal (e.g. chemical doping) or external parameters (such as magnetic and electric fields or strain) [1]. Virtually all states of matter can thus be found in the oxides family (e.g. superconductivity, ferromagnetism, ferroelectricity, etc.), and these states are often highly tunable. This offers immense possibilities for electronic devices, combining, for instance, a conductive or a superconductive oxide as the channel with ferroelectrics in heteroepitaxial ferroelectric field-effect transistors [2]. Magnetic oxides are no less remarkable as they include various half-metallic phases (such as doped manganese perovskites [3]) with

*Author for correspondence (manuel.bibes@thalesgroup.com).

One contribution of 10 to a Discussion Meeting Issue 'The new science of oxide interfaces'.

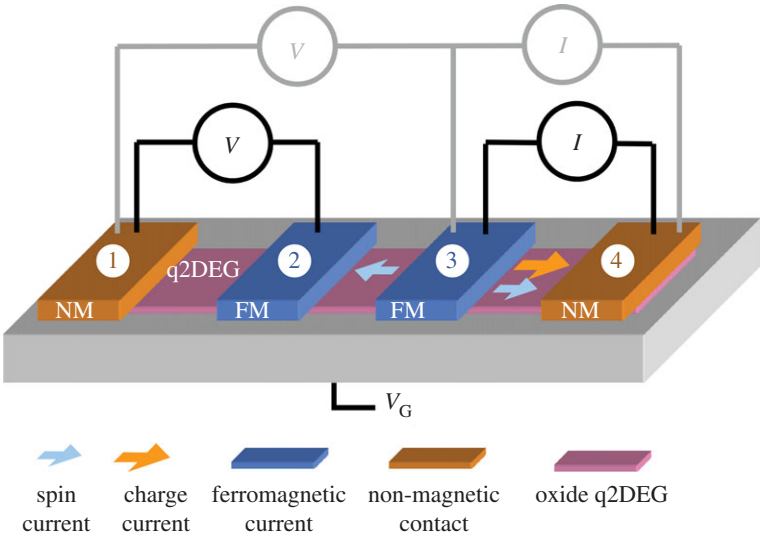

Figure 1. Sketch of a lateral spin valve using an oxide quasi-two-dimensional electron gas (q2DEG) as the channel. The black and grey lines show four- and three-terminal non-local measurement geometries, respectively. (Online version in colour.)

which giant spintronics responses have been obtained. Examples include record tunnel magnetoresistance in $La_{2/3}Sr_{1/3}MnO_3$–$SrTiO_3$–$La_{2/3}Sr_{1/3}MnO_3$ magnetic tunnel junctions [4] or very large spin signals in lateral spin valves combining $La_{2/3}Sr_{1/3}MnO_3$ (LSMO) and carbon nanotubes [5].

2. Motivation

In view of this outstanding ensemble of charge and spin-based phenomena and associated devices, it is tempting to try bridging the gap between gate-controlled lateral charge transport and vertical spin transport in oxide architectures. A prototypical oxide-based device for lateral spin transport is a lateral spin valve that consists of two ferromagnetic contacts (for spin injection and extraction) and an oxide quasi-two-dimensional electron gas (q2DEG) channel to transport spin information. To isolate effects owing to spin transport from other magnetotransport phenomena, such as (tunnel) anisotropic magnetoresistance, it is desirable to separate spin and charge currents by resorting to non-local measurement geometries, as sketched in figure 1. In this device, the charge current injected between contacts 3 and 4 generates a spin current that not only drifts towards 4, but also diffuses towards 2. The spin voltage V between 2 and 1 can thus be detected in a non-local fashion (i.e. independently of the charge voltage). Reversing the magnetization of 2 with respect to that of 3 changes the spin sensitivity and thus the sign of V. A back-gate contact enables a control of the carrier density in the oxide q2DEG and thus of the propagation of the charge and spin currents.

To probe only spin injection and release constraints on the propagation of a spin signal from contacts 3 to 2, a three-terminal (3-T) measurement configuration (shown in grey in figure 1) can be used. Spin injection is then detected via the

depolarizing effect of a perpendicular magnetic field that causes the spin-polarized carriers to undergo Larmor precession (Hanle effect), which progressively destroys the spin accumulation as the field increases [6], see §5.

In practice, to efficiently inject a spin-polarized current into a conductor, an appropriate choice of materials and architectures must be made. One of the usual difficulties resides in the conductivity mismatch between the injecting materials (typically ferromagnetic metals) and the channel materials (typically semiconductors). Several routes are possible to address this issue and achieve an efficient spin injection. One (i) relies on the use of a ferromagnetic injector with roughly the same conductivity as the channel and another (ii) consists of inserting a tunnel barrier between the mismatched injector and channel, which, in some conditions [7], may enable a good spin injection. A third, unexplored route (iii) is based on spin-filtering tunnel barriers [8,9], in which case, the injecting electrode may be a non-magnetic metal. With oxides, all three approaches can be pursued in epitaxial heterostructures combining materials from the same structural families, especially perosvkites. Here, we have pursued route (ii) using as the tunnel barrier the 4–5 unit cell thick $LaAlO_3$ film used to create the q2DEG in adjacent $SrTiO_3$. The conditions for spin injection in our devices will be discussed in §4.

When the spin-injection problem is solved, four-contact non-local spin detection in lateral spin valves may be attempted. For a finite spin signal to be detected, the dwell time of the spin-polarized electrons between the ferromagnetic injection and detection contacts must be shorter than the spin lifetime τ_{sf}. Practically, this implies that the distance between these two contacts must be shorter than the spin diffusion length and that the detection contact must be transparent enough to facilitate the extraction of the spin-polarized electrons. This thus imposes strict conditions on both the channel material and the interface between the channel and the detection contact. Although no τ_{sf} values are available for oxide-based channel materials, the recent discovery of high-mobility two-dimensional electron systems in ZnO quantum wells [10,11], at interfaces between two insulating perovskites oxides such as $LaAlO_3$ and $SrTiO_3$ (STO) (LAO–STO) [12–15] and in lightly doped STO thin films [16,17] brings hopes of relatively long τ_{sf} values.

In the future, lateral spintronics devices based on oxide materials could eventually benefit from the outstanding multi-functional properties of transition-metal oxides and may open the way towards spin transistors with multiple degrees of freedom, fully controllable by electric fields. As in the case of magnetic tunnel junctions, changing the magnetic configuration of the ferromagnetic contacts from parallel to antiparallel in lateral spin valves is usually achieved by applying a magnetic field (figure 2*a*). Taking advantage of the recent progress in artificial multi-ferroic tunnel junctions [18], it should be feasible to change the effective spin polarization of the contacts by an electric field using ferroelectrics (figure 2*b*). Inserting a ferroelectric tunnel barrier between the ferromagnetic contacts and the channel could not only result in the depletion/accumulation of charge carriers in the channel close to the ferroelectric, but also change the injected spin polarization [19]. Both phenomena will enable a non-volatile electric-field control of spin injection in the device.

Another possibility to control the spin polarization of the ferromagnetic contacts without modifying the electrical conditions for spin injection and detection could consist of exploiting the magnetoelectric effect between the

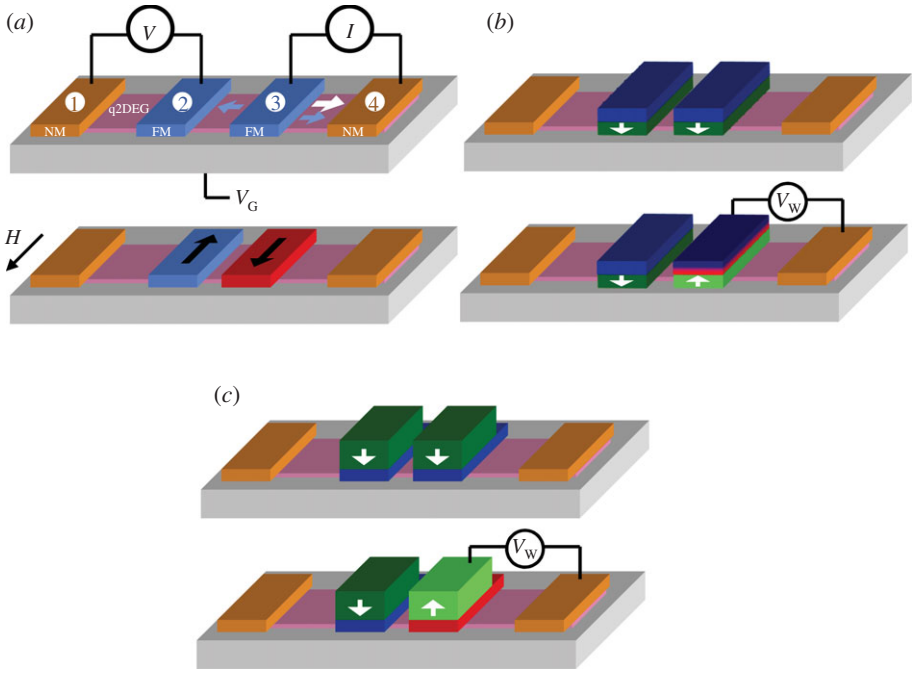

Figure 2. Lateral spin valves in which the spin polarization of the injected current is switched by (*a*) a magnetic field, (*b*) the ferroelectric modification of the interfacial spin polarization and (*c*) the magnetoelectric modification of the contacts magnetization via the application of a write voltage V_w. The ferroelectric polarization in the ferroelectric layers is shown by vertical white arrows. (Online version in colour.)

ferromagnetic contacts and a multi-ferroic [20,21] or piezoelectric [22] grown on top, in order to control the orientation of the ferromagnets' magnetization (and as a result, the effective spin polarization), figure 2*c*. In addition, oxides can also provide advanced gating schemes using ferroelectrics, ferromagnetic insulators or multi-ferroics to manipulate spin information between the injection and detection contacts. In view of this world of possibilites, it is clear that besides their strong interest for electronics [23,24], oxide q2DEGs are exciting for the exploration of novel spintronics phenomena in multi-functional heterostructures.

In this paper, we describe the fabrication of spin-injection devices based on an LAO–STO q2DEG and report magnetotransport data that suggest electrical spin injection into the LAO–STO interface. Because the spin diffusion length of this system is unknown, we resort to a three-terminal measurement geometry with only one ferromagnetic tunnel contact and focus on spin injection [25], essential for future lateral spin valves based on this system. This 3-T geometry has recently been employed to probe the spin-injection efficiency in semiconductor channels [6,26–32]. Spin injection is then detected through a correlated change of the spin splitting and voltage at the interface between the tunnel contact and the channel. Here, through combined 3-T Hanle measurements in both Voigt ($H_\perp$) and Faraday ($H_\parallel$) geometries, we present evidence of electrical spin injection into oxide-based FM–$LaAlO_3$–$SrTiO_3$ junctions, where FM is a 3d ferromagnet such as Co.

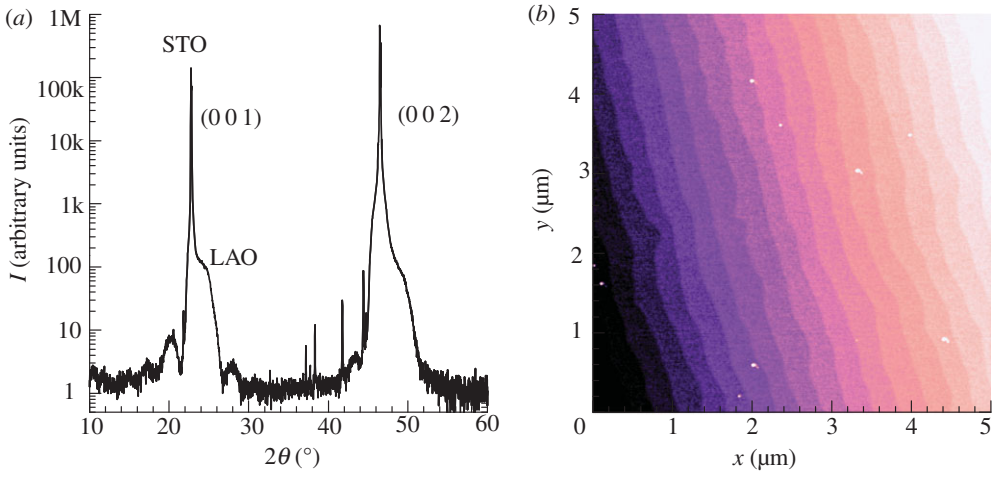

Figure 3. (*a*) Standard 2θ–ω diffractogram of a 9 unit cell LAO film. Finite-size (Laue) fringes are observed. The sharp extra peaks are due to the absence of a monochromator to filter spurious radiations lines in addition to Cu K_α. (*b*) Atomic force microscopy (AFM) image of a 4 unit cell sample. The colour scale (height) range is 7 nm, the step height is 1 unit cell. (Online version in colour.)

3. Sample preparation

Films of LAO 4–5 unit cells thick were deposited by pulsed laser deposition on a TiO_2-terminated STO substrate, heated between 650 and 750°C, in an oxygen pressure of 10^{-4} mbar. The KrF excimer laser (248 nm) is incident on the LAO single-crystal target with a fluence of 0.6–1.2 J cm^{-2} at 1 Hz frequency, leading to a deposition rate of about 1 unit cell per minute on the substrate. The substrate–target distance is 77 mm. After deposition, the oxygen pressure in the deposition chamber is increased to about 0.7 bar, the temperature lowered to 500–550°C and kept in these conditions for 60 min in order to reoxygenate the STO substrate and avoid oxygen vacancies [33]. Eventually, the sample is cooled down to room temperature in 1 h. Figure 3*a* shows an X-ray diffraction $2\theta - \omega$ scan of a 9 unit cell thick LAO film that clearly displays Laue fringes adjacent to the main (0 0 1) and (0 0 2) diffraction peaks, attesting the high structural coherence of the LAO. The obtained films are atomically flat, with the characteristic step-and-terrace morphology (figure 3*b*), each step being 1 unit cell high.

Prior to epitaxial LAO deposition, the substrate was patterned by a UV photoresist mask used to lift off an amorphous LAO layer deposited at room temperature, a technique inspired by Schneider *et al.* [34]. These amorphous areas remained insulating after the deposition of the film at high temperature, allowing us to pattern a well-defined channel. Photolithography and lift-off were also used to produce the FM electrodes, which were deposited by DC magnetron sputtering at room temperature. For the cobalt FM electrodes, a 15–50 nm gold layer was deposited *in situ* on top to avoid the oxidation of the thin FM layers that were 15 nm thick. Figure 4*a* shows an atomic force microscopy (AFM) image of the device near the interface between the channel and the Co–Au contacts.

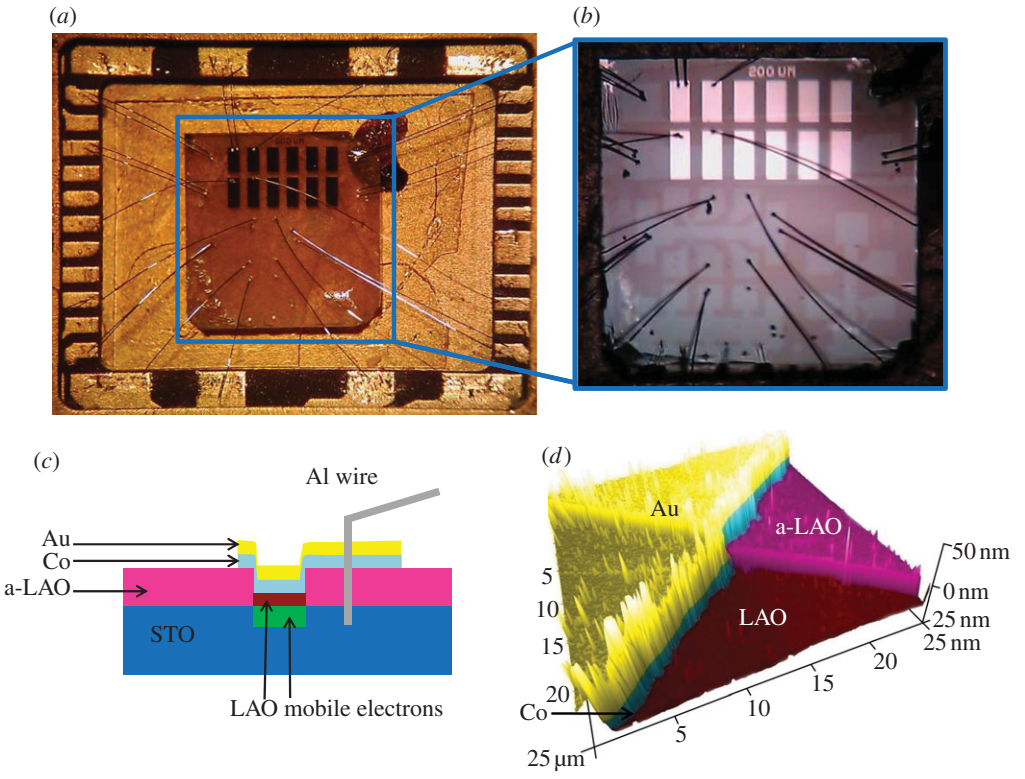

Figure 4. (*a*) False colour AFM image of the device after channel and top electrode definition. (*b*) Sketch of the device in cross section. (*c*,*d*) Optical photographs of the device after wire bonding. Below the spin-injection device (top part), Hall bars are also visible. (Online version in colour.)

The Co-based electrode film was kept thin enough in order to maintain as much as possible of its magnetization in-plane, allowing observation of the Hanle effect before the reorientation of the electrode at larger magnetic fields.

Aluminum wire ultrasound welding was used to contact the FM electrodes and the channel ensuring ohmic contacts with the q2DEG at the LAO–STO interface as well as with the FM electrodes, see the sketch in figure 4*b*. The typical size of the tunnelling contacts patterned by UV lithography for I–V and Hanle measurements was $100 \times 300\,\mu m^2$. Figure 4*c*,*d* shows optical images of the final device after wire bonding into the chip carrier. The resistances were mainly measured using a current source (Keithley 6220 or 6221) and a nanovoltmeter (Keithley 2182A). The field effect was applied with a voltage source that allowed the leakage current to be monitored (Keithley 2400).

4. Conditions for spin injection

As discussed by several authors including Fert *et al.* [25], the efficient spin injection from a ferromagnetic metal into a semiconducting channel requires the introduction of a finite spin-conserving resistance at the interface between

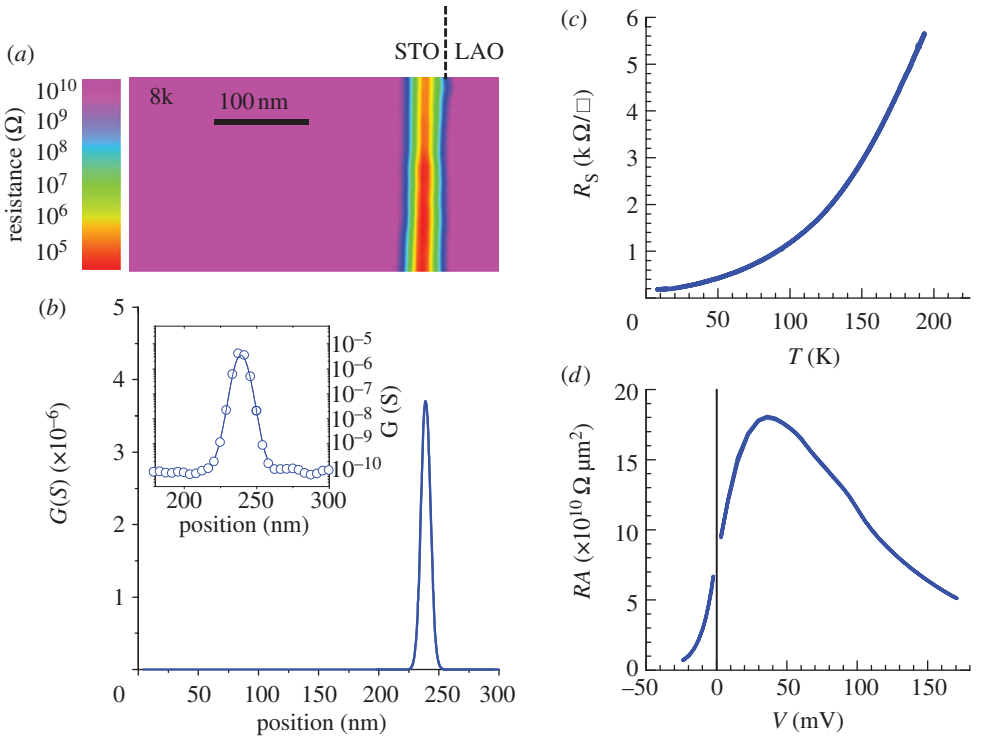

Figure 5. (*a*) Cross-sectional CTAFM resistance mapping of a 5 unit cell LAO film on STO at 8 K. (*b*) Resistance profile across the LAO–STO interface extracted from (*a*). Adapted from Copie *et al.* [38]. (*c*) Temperature dependence of the sheet resistance of the LAO–STO channel in the device. (*d*) Bias dependence of the resistance-area product between the Co injection contact and an ohmic Al contact on the LAO–STO channel at 12 K for a 100 × 300 μm^2 junction. (Online version in colour.)

the ferromagnet and the channel. Practically, tunnel contacts can prove efficient for this purpose as direct tunnelling is a spin-conserving process. Quantitatively and in the case of spin injection from a Co electrode into an LAO–STO q2DEG, the spin polarization of the injected current can be expressed as

$$P_{\mathrm{int}} = \frac{\beta r_{\mathrm{Co}} + \gamma r_b^{\star}}{r_{\mathrm{Co}} + r_{2-D} + r_b^{\star}} \tag{4.1}$$

with β and γ the spin polarization in Co and at the LAO–Co interface, respectively, r_{Co} and $r_{2-D} = R_{\mathrm{S}} l_{\mathrm{sf}}^2$ the (unit area) spin resistance of the Co electrode and of the q2DEG (with R_{S} the channel sheet resistance and l_{sf} the spin diffusion length) and $r_b^{\star}$ the interface resistance area product.

Practically, $r_b^{\star}$ is likely to be much larger than r_{Co} so that the numerator of equation (4.1) can be approximated by $\gamma r_b^{\star}$. For the LAO–Co interface, γ was measured by Garcia *et al.* [35] in LSMO–LAO–Co magnetic tunnel junctions showing negative tunnel magnetoresistance of about −20 per cent at low temperature. Using Julliere's formula [36] and a spin polarization of +90 per cent for LSMO [37], one estimates $\gamma = -0.1$. r_{2-D} can be estimated from

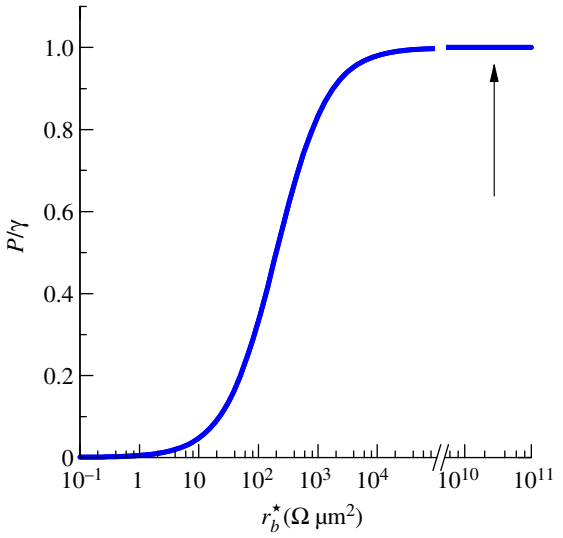

Figure 6. Dependence of the relatively injected spin polarization as a function of the interface resistance. (Online version in colour.)

the sheet resistance that we plot in figure 5*c* as a function of temperature and the thickness of the q2DEG. Assuming a spin diffusion length $l_{sf} = 1\,\mu m$ and taking the value of $R_S = 200\,\Omega$ at 12 K yields $r_{2-D} = 200\,\Omega\,\mu m^2$. Importantly, the thickness of the q2DEG is here much lower than l_{sf}, thereby preventing spin depolarization normal to the q2DEG plane. The q2DEG thickness was measured directly by conductive-tip AFM at low temperature in cross-section samples, as reported by Basletic *et al.* [13] and Copie *et al.* [38] and presented in figure 5*a*,*b*. From the conductive tip atomic force microscopy (CTAFM) image, it can be appreciated that the q2DEG is confined over a finite thickness close to the LAO–STO interface. The full width at half maximum of the resistance profile (figure 5*b*) indicates a thickness of 12 nm.

Using the above parameters, we can plot the injected spin polarization as a function of the interface resistance $r_b^\star$ (figure 6). Values in excess of $10^4\,\Omega\mu m^2$ are required to achieve optimal efficiency. Experimentally, the interface resistance is much larger than this threshold value, as visible from figure 5*d*, which plots the resistance between the Co injection contact and an ohmic Al contact on the LAO–STO channel as a function of measurement voltage. The arrow in figure 6 indicates this experimental value. From this analysis, we conclude that in a direct tunnelling spin-injection regime, an optimally spin-polarized current should be injected from Co into the LAO–STO q2DEG.

5. Magnetotransport measurements

Insight into the transport mechanism at play in the device is already provided by the typical tunnelling resistance versus bias curve shown in figure 5*d*, showing a clear asymmetry between positive and negative bias, reminiscent of previous observations for Au and Pt reference electrodes in Singh-Bhalla *et al.* [39]. This

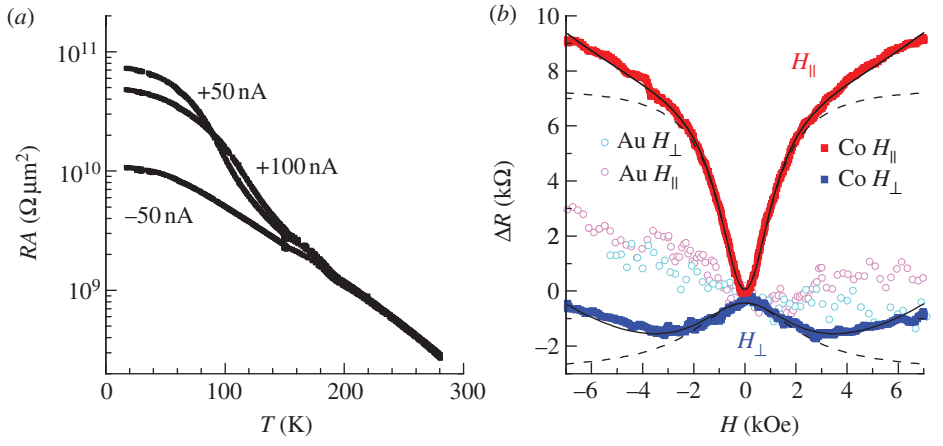

Figure 7. (*a*) Temperature dependence of the *RA* product measured at injected currents of $I = +100, +50$ and -50 nA. (*b*) Magnetoresistance as a function of magnetic field (solid squares) with the field applied perpendicular (Hanle effect) and parallel (inverse Hanle effect) to the sample plane, at 2 K. The solid lines are fits with a Lorentzian plus a parabolic background and the dashed lines show only the Lorentzian contribution due to the Hanle effect. Magnetoresistance at an Au tunnel contact is shown for comparison (open symbols). Adapted from Reyren *et al.* [41]. (Online version in colour.)

asymmetry mainly originates from the strong trapezoidal shape of the LAO barrier caused by the difference of the materials' workfunctions. The bias electric field needed to achieve measurable currents probably influences the q2DEG carrier concentration by the field effect [24,40], which considerably complicates the analysis of the corresponding I–V curves that we thus do not attempt to fit.

In contrast to the channel sheet resistance that *decreases* with temperature (figure 5*c*), we have found that the resistance of Co–$LaAlO_3$–$SrTiO_3$ junctions strongly *increases* with temperature, in a thermally activated way (figure 7*a*). Data acquired at positive current (electrons injected from the q2DEG towards the FM electrode) display a very strong temperature dependence and the *RA* product increases by almost three orders of magnitude from 300 to 10 K. This is a clear signature of inelastic tunnelling transport processes through localized states (LSs) embedded in the LAO barrier. We infer that these LSs are partitioned in LAO at the LAO–STO interface with characteristic occupation energy levels close to the Fermi level of the q2DEG in STO. Owing to the band structure, articulation at LAO–STO interfaces highlighted by *in situ* photoemission [42] and to the position of the electronic level of intrinsic defects in LAO calculated by density-functional theory (DFT) [43,44], such LSs are probably played by oxygen vacancies or intermixing [45,46] in LAO. This leads to available electronic states accessible for spin injection at 3s−3p Al or 6s−5d La on-site orbitals. Other different point defects in LAO, such as ionized interstitial Al^{3+} or La^{3+}, are also possible candidates [43]. This is discussed further later.

We now turn on to Hanle magnetoresistance data. Figure 7*b* shows a typical 3-T Hanle signal, acquired at 2 K and at positive current $I = +50$ nA (+0.13 V bias), in standard Voigt geometry (field perpendicular to the plane $H_{\perp}$) and Faraday geometry (field in the plane $H_{\|}$) [41]. Aside from a superimposed parabolic background, the $H_{\perp}$ curve displays a quasi-Lorentzian shape of about

$2\,\mathrm{k}\Omega$ ($60\,\mathrm{M}\Omega\,\mu\mathrm{m}^2$ of resistance area) amplitude compared with the base $2.7\,\mathrm{M}\Omega$ ($80\,\mathrm{G}\Omega\,\mu\mathrm{m}^2$, figure 5*d*) resistance, which is a total magnetoresistance of 0.7 per cent. This negative magnetoresistance evidences a correlated drop of the spin splitting $\Delta\mu = \mu_\uparrow - \mu_\downarrow$ (with $\mu_{\uparrow,\downarrow}$ the respective electrochemical potential for spin $\uparrow,\downarrow$) and voltage ΔV according to $\Delta V = \gamma\Delta\mu/(2e)$ [47,48], where e is the electronic charge. A primary analysis leads to a splitting of the chemical potential $\Delta\mu(H)$ of the form $\Delta\mu(0)/[1 + (\omega_\mathrm{L}\tau_\mathrm{sf})^2]$, where ω_L is the Larmor frequency, and a characteristic spin-relaxation time τ_sf can be extracted from the width of the Lorentzian. Correspondingly, the magnetoresistance curves (figure 7*b*) are fitted by $R(H) = R(0)/[1 + (\omega_\mathrm{L}\tau_\mathrm{sf})^2]$ plus a parabolic background, where $\omega_\mathrm{L} = g_e\mu_\mathrm{B}H/\hbar$ is calculated by assuming a Landé factor g_e=2. Using such a procedure, we would extract a typical value of $\tau_\mathrm{sf} = 50\,\mathrm{ps}$ at 2 K. Considering a diffusion constant $\mathcal{D} \simeq 40\,\mathrm{cm}^2\,\mathrm{s}^{-1}$ [49], this corresponds to a spin-diffusion length $\ell_\mathrm{sf} = \sqrt{\mathcal{D}\tau_\mathrm{sf}} \approx 1\,\mu\mathrm{m}$. Nevertheless, alternative mechanisms of spin depolarization caused by random magnetic fields may modify the Hanle signals as well as artificially enlarging the width of the Lorentzian shape [30].

In order to go beyond this first simple analysis, figure 7*b* also presents the results of Hanle experiments in a Faraday geometry where the magnetic field was applied along the direction of the injected spins. In the field scale limit of $\sim 0.7\,\mathrm{T}$, a total Hanle (normal plus inverted) signal ΔR_H of about $10\,\mathrm{k}\Omega$ ($0.3\,\mathrm{G}\Omega\,\mu\mathrm{m}^2$) is measured before reorientation of the Co magnetization occurring around 1.8 T (not shown). Striking similarities with the signals obtained at FM–AlO_2–Si junctions [30] suggest that common mechanisms of spin injection occur in these systems and thus explain a *negative* peak (inverted Hanle curve) in the magnetoresistance data. This may originate from the presence of a random magnetic field causing precession and loss of spin accumulation. In other words, the application of a transverse magnetic field results in a loss of spin coherence, while an external field applied parallel to the injected spin restores the spin accumulation. Therefore, ΔR_H should scale with the total amplitude of spin accumulation at the LAO–STO interface. However, we note that this spin signal is enhanced by more than *five orders of magnitude* compared with intrinsic spin resistance $R^s_\mathrm{ch} = R_\square \times l^2_\mathrm{sf}$ of the q2DEG evaluated at approximately $100\,\Omega\,\mu\mathrm{m}^2$ for a typical l_sf of $1\,\mu\mathrm{m}$, indicating that some highly efficient amplification process is at play, as in Tran *et al.* [26]. Further experiments on the influence of the bias and gate voltage can shed light on this phenomenon [41].

We now discuss in more detail the possible origin of the random field, including the stray field [30], the Rashba spin–orbit field [49,50] and hyperfine interactions [51,52], responsible for spin decoherence. In the present case, one can easily discard stray field effects as the LAO surface is atomically flat, with only 1 unit cell steps (approx. 4 Å) over 200 nm wide terraces. On the other hand, Rashba spin–orbit interactions [49,50] are known to vanish on (non-propagative) LSs. More likely, as for the case of hybrid organic spin valves [53] or ZnO oxide quantum dots [54], the random field may have a hyperfine origin, Al^{3+} and La^{3+} sites (Al or La antisites or bounded to oxygen vacancies) bearing, respectively, a nuclear moment of $I_\mathrm{Al} = \frac{5}{2}$ for ^{27}Al (with 100% abundance) and $I_\mathrm{La} = \frac{7}{2}$ for ^{139}La (with 99.91% abundance). In this scenario, electrons are subject to a nuclear field [51,55],

$$H_\mathrm{n} = \tfrac{2}{3}\mu_0 g_\mathrm{n}\mu_\mathrm{B}\hbar \boldsymbol{I}\cdot\boldsymbol{S}|\psi(0)|^2,$$

where g_n is the nuclear gyromagnetic ratio ($g_n^{Al} = 1.4566$, $g_n^{La} = 0.7952$) and $\psi(0)$ is the weight of their respective 3s- and 6s-type wavefunctions at the centre. Taking into account the respective value for g_n, a good estimate of the nuclear field for both Al and La is about 0.1–0.2 T, taking into account the typical extension of their wavefunctions [56]. In an inverted Hanle experiment (Faraday geometry), and in the limit of a long spin lifetime, the voltage drop ΔV measured at a junction equals $\Delta V = (\gamma/2)\Delta\mu/e\langle\cos^2(\theta)\rangle$ [30], where θ is the angle between the spin and the effective magnetic field, which itself is the sum of the random nuclear fields, H_n and the external field H. The resistance variation $\Delta R_H \propto \langle\cos^2(\theta_H)\rangle$ slightly departs from a standard Lorentzian shape according to the formula (see Figure 7.)

$$\Delta R_H(H_{||}) \propto \frac{3}{4} - \frac{1}{4h^2} + \frac{(1-h^2)^2}{8h^3} \ln\left|\frac{1+h}{1-h}\right|, \tag{5.1}$$

where h is the reduced field $H_{||}/H_n$. The total amplitude of the inverted Hanle effect is then $\frac{2}{3}$ of the total amplitude of $\Delta R_H = \gamma\Delta\mu/2j$. This corresponds to a gradual restoration of the spin accumulation in proportion $\frac{2}{3}$, while the normal Hanle effect has a proportion of $\frac{1}{3}$ as one can expect. Then, the particular value of the external field $H_{1/4}$, corresponding to $h = 1$ and for which $\Delta R_H(H_{1/4}) = \frac{3}{4}\Delta R_H(0) + \frac{1}{4}\Delta R_H(H_\infty)$, gives the magnitude of the random field that lies around 0.1 T, in agreement with the estimation of the nuclear field of Al and La given above.

6. Conclusion

In conclusion, we have investigated spin injection from a magnetic tunnel contact towards the $LaAlO_3$–$SrTiO_3$ two-dimensional electron system by using a three-terminal Hanle approach in both Voigt and Faraday geometries. Both the Hanle and inverted Hanle signals are strongly enhanced, consistent with amplification effects by LSs positioned in the $LaAlO_3$ barrier midgap, possibly associated with oxygen vacancies or intermixing. We propose that the inverted Hanle effect is due to spin depolarization by random nuclear fields. In order to detect the direct injection of spin-polarized carriers into the $LaAlO_3$–$SrTiO_3$ channel, either the injection contact resistance must be significantly reduced, for instance, by replacing $LaAlO_3$ with a lower gap material, or four-contact non-local detection schemes must be implemented. This would require distances between the injector and detector smaller than the characteristic spin-diffusion length, which should be achievable with electron-beam lithography techniques. Resorting to lightly doped $SrTiO_3$ films with higher electron mobilities may be another way to reduce the constraints on channel dimensions.

We thank E. Jacquet and R. Bernard for technical help with the pulsed laser deposition (PLD) set-up. We acknowledge financial support from the French Agence Nationale de la Recherche (project 'Oxitronics') and the Triangle de la Physique (project 'Easox').

References

1 Dagotto, E. 2005 Complexity in strongly correlated electronic systems. *Science* **309**, 257–262. (doi:10.1126/science.1107559)

2 Ahn, C. H. *et al.* 2006 Electrostatic modification of novel materials. *Rev. Mod. Phys.* **78**, 1185–1212. (doi:10.1103/RevModPhys.78.1185)
3 Coey, J. M. D., Viret, M. & von Molnàr, S. 1999 Mixed-valence manganites. *Adv. Phys.* **58**, 167–293. (doi:10.1080/000187399243455)
4 Bowen, M., Bibes, M., Barthélémy, A., Contour, J. P., Anane, A., Lemaître, Y. & Fert, A. 2003 Nearly total spin polarization in $La_{2/3}Sr_{1/3}MnO_3$ from tunneling experiments. *Appl. Phys. Lett.* **82**, 233–235. (doi:10.1063/1.1534619)
5 Hueso, L. E. *et al.* 2007 Transformation of spin information into large electrical signals using carbon nanotubes. *Nature* **445**, 410–413. (doi:10.1038/nature05507)
6 Lou, X., Adelmann, C., Furis, M., Crooker, S. A., Palmstrøm, C. J. & Crowell, P. A. 2006 Electrical detection of spin accumulation at a ferromagnet-semiconductor interface. *Phys. Rev. Lett.* **96**, 176603. (doi:10.1103/PhysRevLett.96.176603)
7 Fert, A. & Jaffrès, H. 2001 Conditions for efficient spin injection from a ferromagnetic metal into a semiconductor. *Phys. Rev. B* **64**, 184420. (doi:10.1103/PhysRevB.64.184420)
8 Gajek, M., Bibes, M., Barthélémy, A., Bouzehouane, K., Fusil, S., Varela, M., Fontcuberta, J. & Fert, A. 2005 Spin filtering through ferromagnetic $BiMnO_3$ tunnel barriers. *Phys. Rev. B* **72**, 020406. (doi:10.1103/PhysRevB.72.020406)
9 Luders, U. *et al.* 2006 Spin filtering through ferrimagnetic $NiFe_2O_4$ tunnel barriers. *Appl. Phys. Lett.* **88**, 082505. (doi:10.1063/1.2172647)
10 Ghosh, S., Sih, V., Lau, W. H., Awschalom, D. D., Bae, S.-Y., Wang, S., Vaidya, S. & Chapline, G. 2005 Room-temperature spin coherence in ZnO. *Appl. Phys. Lett.* **86**, 232507. (doi:10.1063/1.1946204)
11 Tsukazaki, A., Akasaka, S., Nakahara, K., Ohno, Y., Ohno, H., Maryenko, D., Ohtomo, A. & Kawasaki, M. 2010 Observation of the fractional quantum Hall effect in an oxide. *Nat. Mater.* **9**, 889–893. (doi:10.1038/nmat2874)
12 Ohtomo, A. & Hwang, H. Y. 2004 A high-mobility electron gas at the $LaAlO_3/SrTiO_3$ heterointerface. *Nature* **427**, 423–426. (doi:10.1038/nature02308)
13 Basletic, M., Maurice, J. L., Carrétéro, C., Herranz, G., Copie, O., Jacquet, E., Bouzehouane, K., Fusil, S. & Barthélémy, A. 2008 Mapping the spatial distribution of charge carriers in $LaAlO_3/SrTiO_3$ heterostructures. *Nat. Mater.* **7**, 621–625. (doi:10.1038/nmat2223)
14 Caviglia, A. D., Gariglio, S., Cancellieri, C., Sacépé, B., Fête, A., Reyren, N., Gabay, M., Morpurgo, A. F. & Triscone, J.-M. 2010 Two-dimensional quantum oscillations of the conductance at $LaAlO_3/SrTiO_3$ interfaces. *Phys. Rev. Lett.* **105**, 236802. (doi:10.1103/PhysRevLett.105.236802)
15 Ben Shalom, M., Ron, A., Palevski, A. & Dagan, Y. 2010 Shubnikov-de Haas oscillations in $SrTiO_3/LaAlO_3$ interface. *Phys. Rev. Lett.* **105**, 206401. (doi:10.1103/PhysRevLett.105.206401)
16 Kozuka, Y., Kim, M., Bell, C., Kim, B. G., Hikita, Y. & Hwang, H. Y. 2009 Two-dimensional normal-state quantum oscillations in a superconducting heterostructure. *Nature* **462**, 487–490. (doi:10.1038/nature08566)
17 Son, J., Moetakef, P., Jalan, B., Bierwagen, O., Wright, N. J., Engel-Herbert, R. & Stemmer, S. 2010 Epitaxial $SrTiO_3$ films with electron mobilities exceeding $30\,000\,cm^2\,V^{-1}\,s^{-1}$. *Nat. Mater.* **9**, 482–484. (doi:10.1038/nmat2750)
18 Garcia, V. *et al.* 2010 Ferroelectric control of spin polarization. *Science* **327**, 1106–1110. (doi:10.1126/science.1184028)
19 Zhuravlev, M. Y., Jaswal, S. S., Tsymbal, E. Y. & Sabirianov, R. F. 2005 Ferroelectric switch for spin injection. *Appl. Phys. Lett.* **87**, 222114. (doi:10.1063/1.2138365)
20 Bibes, M. & Barthélémy, A. 2008 Towards a magnetoelectric memory. *Nat. Mater.* **7**, 425–426. (doi:10.1038/nmat2189)
21 Wu, S. M., Cybart, S. A., Yu, P., Rossell, M. D., Zhang, J. X. Ramesh, R. & Dynes, R. C. 2010 Reversible electric control of exchange bias in a multiferroic field-effect device. *Nat. Mater.* **9**, 756–761. (doi:10.1038/nmat2803)
22 Weiler, M. *et al.* 2009 Voltage controlled inversion of magnetic anisotropy in a ferromagnetic thin film at room temperature. *New J. Phys.* **11**, 013021. (doi:10.1088/1367-2630/11/1/013021)
23 Cen, C., Thiel, S., Mannhart, J. & Levy, J. 2009 Oxide nanoelectronics on demand. *Science* **323**, 1026–1030. (doi:10.1126/science.1168294)

24 Jany, R. *et al.* 2010 Diodes with breakdown voltages enhanced by the metal-insulator transition of $LaAlO_3$–$SrTiO_3$ interfaces. *Appl. Phys. Lett.* **96**, 183504. (doi:10.1063/1.3428433)

25 Fert, A., George, J.-M., Jaffrès, H. & Mattana, R. 2007 Semiconductors between spin-polarized sources and drains. *IEEE Trans. Electron Dev.* **54**, 921–932. (doi:10.1109/TED.2007.894372)

26 Tran, M., Jaffrès, H., Deranlot, C., George, J.-M., Fert, A., Miard, A. & Lemaître, A. 2009 Enhancement of the spin-accumulation at the interface between a spin-polarized tunnel junction and a semiconductor. *Phys. Rev. Lett.* **102**, 036601. (doi:10.1103/PhysRevLett.102.036601)

27 Dash, S. P., Sharma, S., Patel, R. S., de Jong, M. P. & Jansen, R. 2009 Electrical creation of spin polarization in silicon at room temperature. *Nature* **462**, 491–494. (doi:10.1038/nature08570)

28 Sazaki, T., Oikawa, T., Suzuki, T., Shiraishi, M., Suzuki, Y. & Noguchi, K. 2010 Comparison of spin signals in silicon between nonlocal four-terminal and three-terminal methods. *Appl. Phys. Lett.* **96**, 122101. (doi:10.1063/1.3367748)

29 Suzuki, T., Sazaki, T., Oikawa, T., Shiraishi, M., Suzuki, Y. & Noguchi, K. 2011 Room-temperature electron spin transport in a highly doped Si channel. *Appl. Phys. Express* **4**, 023003. (doi:10.1143/APEX.4.023003)

30 Dash, S. P., Sharma, S., Le Breton, J. C., Peiro, J., Jaffrès, H. George, J.-M., Lemaître, A. & Jansen, R. 2011 Spin precession and decoherence near an interface with a ferromagnet. *Phys. Rev. B* **84**, 054410. (doi:10.1103/PhysRevB.84.054410)

31 Li, C. H., van't Erve, O. M. J. & Jonker, B. T. 2011 Electrical injection and detection of spin accumulation in silicon at 500 K with magnetic metal/silicon dioxide contacts. *Nat. Commun.* **2**, 245. (doi:10.1038/ncomms1256)

32 Ando, Y. *et al.* 2011 Bias current dependence of spin accumulation signals in a silicon channel detected by a Schottky tunnel contact. *Appl. Phys. Lett.* **99**, 012113. (doi:10.1063/1.3607480).

33 Cancellieri, C. *et al.* 2010 Influence of the growth conditions on the $LaAlO_3/SrTiO_3$ interface electronic properties. *Europhys. Lett.* **91**, 17004. (doi:10.1209/0295-5075/91/17004)

34 Schneider, C. W., Thiel, S., Hammerl, G., Richter, C. & Mannhart, J. 2006 Microlithography of electron gases formed at interfaces in oxide heterostructures. *Appl. Phys. Lett.* **89**, 122101. (doi:10.1063/1.2354422)

35 Garcia, V., Bibes, M., Maurice, J. L., Jacquet, E., Bouzehouane, K., Contour, J. P. & Barthélémy, A. 2005 Spin-dependent tunneling through high-k $LaAlO_3$. *Appl. Phys. Lett.* **87**, 212501. (doi:10.1063/1.2132526)

36 Julliere, M. 1975 Tunneling between ferromagnetic films. *Phys. Lett. A* **54**, 225–226. (doi:10.1016/0375-9601(75)90174-7)

37 Garcia, V., Bibes, M., Barthélémy, A., Bowen, M., Jacquet, E., Contour, J. P. & Fert, A. 2004 Temperature dependence of the interfacial spin polarization of $La_{2/3}Sr_{1/3}MnO_3$. *Phys. Rev. B* **69**, 052403. (doi:10.1103/PhysRevB.69.052403)

38 Copie, O. *et al.* 2009 Towards two-dimensional metallic behavior at $LaAlO_3/SrTiO_3$ interfaces. *Phys. Rev. Lett.* **102**, 216804. (doi:10.1103/PhysRevLett.102.216804)

39 Singh-Bhalla, G., Bell, C., Ravichandran, J., Siemons, W., Hikita, Y., Salahuddin, S., Hebard, A. F., Hwang, H. Y. & Ramesh, R. 2011 Built-in and induced polarization across $LaAlO_3/SrTiO_3$ heterojunctions. *Nat. Phys.* **7**, 80–86. (doi:10.1038/nphys1814)

40 Thiel, S., Hammerl, G., Schmehl, A., Schneider, C. W. & Mannhart, J. 2006 Tunable quasi-two-dimensional electron gases in oxide heterostructures. *Science* **313**, 1942–1945. (doi:10.1126/science.1131091)

41 Reyren, N., Bibes, M., Lesne, E., George, J.-M., Deranlot, C., Collin, S., Barthélémy, A. & Jaffrès. H. 2012 Gate-controlled spin injection at $LaAlO_3/SrTiO_3$ interfaces. *Phys. Rev. Lett.* **108**, 186802. (doi:10.1103/PhysRevLett.108.186802)

42 Yoshimatsu, K., Yasuhara, R., Kumigashira, H. & Oshima, M. 2008 Origin of metallic states at the heterointerface between the band insulators $LaAlO_3$ and $SrTiO_3$. *Phys. Rev. Lett.* **101**, 026801. (doi:10.1103/PhysRevLett.101.026801)

43 Luo, X., Wang, B. & Zheng, Y. 2009 First-principles study on energetics of intrinsic point defects in $LaAlO_3$. *Phys. Rev. B* **80**, 104115. (doi:10.1103/PhysRevB.80.104115)

44 Zhong, Z., Xu, P. X. & Kelly, P. 2010 Polarity-induced oxygen vacancies at $LaAlO_3/SrTiO_3$ interfaces. *Phys. Rev. B* **82**, 165127. (doi:10.1103/PhysRevB.82.165127)

45 Nakagawa, N., Hwang, H. Y. & Muller, D. A. 2006 Why some interfaces cannot be sharp. *Nat. Mater.* **5**, 204–209. (doi:10.1038/nmat1569)
46 Pauli, S. A. *et al.* 2011 Evolution of the interfacial structure of $LaAlO_3$ on $SrTiO_3$. *Phys. Rev. Lett.* **106**, 036101. (doi:10.1103/PhysRevLett.106.036101)
47 Brattas, A., Bauer, G. E. W. & Kelly, P. J. 2006 Non-collinear magnetoelectronics. *Phys. Rep.* **427**, 157–256. (doi:10.1016/j.physrep.2006.01.001)
48 Barnás, J., Fert, A., Gmitra, M., Weymann, I. & Dugaev, V. K. 2005 From giant magnetoresistance to current-induced switching by spin transfer. *Phys. Rev. B* **72**, 024426. (doi:10.1103/PhysRevB.72.024426)
49 Caviglia, A. D., Gabay, M., Gariglio, S., Reyren, N., Cancellieri, C. & Triscone, J.-M. 2010 Tunable Rashba spin–orbit interaction at oxide interfaces. *Phys. Rev. Lett.* **104**, 126803. (doi:10.1103/PhysRevLett.104.126803)
50 Ben Shalom, M., Sachs, M., Rakhmilevitch, M., Palevski, A. & Dagan, Y. 2010 Tuning spin–orbit coupling and superconductivity at the $SrTiO_3/LaAlO_3$ interface: a magnetotransport study. *Phys. Rev. Lett.* **104**, 126802. (doi:10.1103/PhysRevLett.104.126802)
51 Paget, D., Lampel, G., Sapoval, B. & Safarov, V. I. 1977 Low field electron-nuclear spin coupling in gallium arsenide under optical pumping conditions. *Phys. Rev. B* **15**, 5780–5796. (doi:10.1103/PhysRevB.15.5780)
52 Merkulov, I. A., Efros, A. L. & Rosen, M. 2002 Electron spin relaxation by nuclei in semiconductor quantum dots. *Phys. Rev. B* **65**, 205309. (doi:10.1103/PhysRevB.65.205309)
53 Schoonus, J. J. H. M., Lumens, P. G. E., Wagemans, W., Kohlhepp, J. T., Bobbert, P. A., Swagten, H. J. M. & Koopmans, B. 2009 Magnetoresistance in hybrid organic spin valves at the onset of multiple-step tunneling. *Phys. Rev. Lett.* **103**, 146601. (doi:10.1103/PhysRevLett.103.146601)
54 Liu, W. K. *et al.* 2007 Room-temperature electron spin dynamics in free-standing ZnO quantum dots. *Phys. Rev. Lett.* **98**, 186804. (doi:10.1103/PhysRevLett.98.186804)
55 Millman, S. & Kush, P. 1939 Nuclear spin and magnetic moment of $_{13}Al^{27}$. *Phys. Rev.* **56**, 303–304. (doi:10.1103/PhysRev.56.303)
56 Cowan, R. D. 1981 *The theory of atomic structure and spectra*, ch. 7–8. Berkeley, CA: University of California Press.